


# Wavelength tunable single-mode lasing from cesium lead halide perovskite microwires F

Cite as: Appl. Phys. Lett. **118**, 071103 (2021); <https://doi.org/10.1063/5.0035104>

Submitted: 29 October 2020 . Accepted: 07 January 2021 . Published Online: 16 February 2021

Fangtao Li, Zheng Yang,  Mingming Jiang, Chunfeng Wang, Jianguo Xi, Yufei Zhang,  Caofeng Pan,  Junfeng Lu, and  Rongming Wang

## COLLECTIONS

 This paper was selected as Featured



View Online



Export Citation



CrossMark

## ARTICLES YOU MAY BE INTERESTED IN

[Elliptical micropillar cavity design for highly efficient polarized emission of single photons](#)

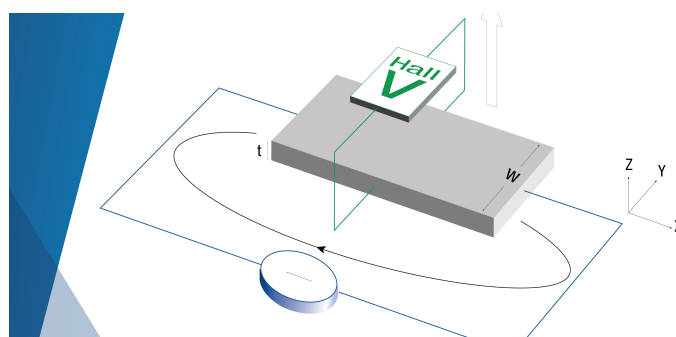
Applied Physics Letters **118**, 061101 (2021); <https://doi.org/10.1063/5.0041565>

[Flat photonics for broadband light-trapping](#)

Applied Physics Letters **117**, 241105 (2020); <https://doi.org/10.1063/5.0033312>

[Conditioning nano-LEDs in arrays by laser-micro-annealing: The key to their performance improvement](#)

Applied Physics Letters **118**, 043101 (2021); <https://doi.org/10.1063/5.0038070>



**Tips for minimizing  
Hall measurement errors**

Download the Technical Note

 **Lake Shore**  
CRYOTRONICS

# Wavelength tunable single-mode lasing from cesium lead halide perovskite microwires

Cite as: Appl. Phys. Lett. **118**, 071103 (2021); doi: [10.1063/5.0035104](https://doi.org/10.1063/5.0035104)

Submitted: 29 October 2020 · Accepted: 7 January 2021 ·

Published Online: 16 February 2021



View Online



Export Citation



CrossMark

Fangtao Li,<sup>1,2</sup> Zheng Yang,<sup>2</sup> Mingming Jiang,<sup>3</sup>  Chunfeng Wang,<sup>3</sup> Jianguo Xi,<sup>2</sup> Yufei Zhang,<sup>2</sup> Caofeng Pan,<sup>2,4,5,6,a)</sup>  Junfeng Lu,<sup>3,a)</sup>  and Rongming Wang<sup>1,a)</sup> 

## AFFILIATIONS

<sup>1</sup>Beijing Advanced Innovation Center for Materials Genome Engineering, Beijing Key Laboratory for Magneto-Photoelectrical Composite and Interface Science, School of Mathematics and Physics, University of Science and Technology Beijing, Beijing 100083, People's Republic of China

<sup>2</sup>CAS Center for Excellence in Nanoscience, Beijing Key Laboratory of Micro-Nano Energy and Sensor, Beijing Institute of Nanoenergy and Nanosystems, Chinese Academy of Sciences, Beijing 100083, People's Republic of China

<sup>3</sup>College of Science, Nanjing University of Aeronautics and Astronautics, Nanjing 210016, People's Republic of China

<sup>4</sup>School of Nanoscience and Technology, University of Chinese Academy of Sciences, Beijing 100049, People's Republic of China

<sup>5</sup>College of Physics and Optoelectronic Engineering, Shenzhen University, Shenzhen 518060, People's Republic of China

<sup>6</sup>Center on Nanoenergy Research, School of Physical Science and Technology, Guangxi University, Nanning, Guangxi 530004, People's Republic of China

<sup>a)</sup>Authors to whom correspondence should be addressed: [cspan@binn.cas.cn](mailto:cspan@binn.cas.cn); [lujunfeng@nuaa.edu.cn](mailto:lujunfeng@nuaa.edu.cn); and [rmwang@ustb.edu.cn](mailto:rmwang@ustb.edu.cn)

## ABSTRACT

Cesium lead halide perovskites have shown great potential applications in photoelectric devices because of their high quantum efficiency, good stability, and tunable bandgap. Herein, we prepared CsPbBr<sub>3</sub> microwires with a high crystal quality, smooth surface, and rectangular cross section via the solution method. The as-prepared microwires presented a high quality whispering gallery mode lasing with a low threshold of 9.1 μJ cm<sup>-2</sup> and a high quality factor of ~3000. Furthermore, we obtained the alloys of CsPbCl<sub>x</sub>Br<sub>3-x</sub> (0 < x < 2) microwires through the gas-phase anion exchange method and realized the wavelength tunable single-mode lasing emission ranging from ~546.8 nm to ~468.0 nm. This work will expand the practical application of lead halide perovskites in spectrograph, optical communication, and in-chip photoelectric devices.

Published under license by AIP Publishing. <https://doi.org/10.1063/5.0035104>

Micro/nanoscale semiconductor lasers with multicolors have exhibited great potential in various commercial fields such as color displays, super-resolution biomedical imaging, and on-chip wavelength-division multiplexing.<sup>1-8</sup> Bandgap engineering and cavity designing are two important ways to obtain multicolor lasers. So far, a lot of achievements have been made based on II-VI and III-V semiconductors through defining the material's composition and nanostructures.<sup>1,9-12</sup> For instance, Kuykendall *et al.* realized the photoluminescence wavelength ranging from 325 nm to 850 nm by controlling the In/Ga ratio in InGaN alloy nanowires (NWs).<sup>13</sup> Yang *et al.* obtained multiwavelength lasing from 517 nm to 636 nm through designing composition-graded CdSse NW nanocavities.<sup>14</sup> However, the high-quality wavelength-tunable single-mode lasing is still desirable for many photoelectric applications, especially for optical communication.

Lead halide perovskites (LHPs) have been considered as ideal materials for photonic and optoelectronic devices due to their outstanding properties such as direct bandgap, high absorption efficiency, tunable wavelength, and high quantum efficiency.<sup>15-18</sup> Compared with organic-inorganic hybrid LHPs, all-inorganic LHPs showed greater potential in laser applications because of their relative stability to moisture, oxygen, light, and heat. In recent years, CsPbX<sub>3</sub> (X = Cl, Br, and I) perovskites and their alloys with various morphologies such as micro/nanowires, sub-microspheres, nanocuboids, nanoplates, and microhemispheres have been widely synthesized by the chemical vapor deposition (CVD) or solution method.<sup>19-26</sup> One of the important merits of LHP-based lasers is that the wavelength can cover the entire visible region through tuning the halide composition. In general, mixed-halide lead perovskites can be acquired by anion exchange due to the typical "soft" crystal lattice characteristic of LHPs.<sup>27,28</sup> Indeed,

organic–inorganic hybrid LHP single/polycrystal NWs with the halide gradient have been prepared by solid–solid or solid–gas anion exchange.<sup>29</sup> Furthermore, CsPbX<sub>3</sub> NW heterojunctions also have been prepared through combined solid–liquid anion exchange and nanofabrication, which provides an opportunity to multicolor lasers or LEDs.<sup>20</sup> Following that, Pan *et al.* obtained the halide axial concentration gradients CsPbCl<sub>x</sub>Br<sub>3-x</sub> NWs by constructing CsPbCl<sub>3</sub> microplate heterojunctions with CsPbBr<sub>3</sub> NWs and carefully studied their halide ion migration dynamics.<sup>30</sup> More recently, dual-color and multicolor lasers were obtained from single composition-graded CsPbBr<sub>x</sub>I<sub>3-x</sub> NWs via CVD, respectively.<sup>2,31</sup> In addition to the remarkable achievements, gas-phase anion exchange has been considered as a prospective method for precisely regulating the halide composition in LHPs by controlling the reaction time and the monitoring the fluorescence microscope.<sup>32</sup> For example, He *et al.* obtained multicolor lasers from CsPbCl<sub>x</sub>Br<sub>3-x</sub> microdisks by controlling solid–gas reaction time.<sup>33</sup> Yang *et al.* realized halide exchange in large area perovskite single crystal films through the gas-phase anion exchange reaction.<sup>16</sup> Single crystal CsPbBr<sub>3</sub> MWs with a rectangular cross section provide a platform for high quality whispering-gallery-mode (WGM) lasers.<sup>15,34</sup> In the last year, Yang *et al.* prepared CsPbBr<sub>3</sub> MW arrays and realized lasing mode dynamic regulation in about 10 nm range.<sup>15</sup> Meanwhile, they have extremely high practical application values for realizing a wide range of tunable single-mode lasing outputs.

In this work, we fabricated CsPbBr<sub>3</sub> MWs via the solution method. The as-prepared CsPbBr<sub>3</sub> MWs showed a smooth surface,

rectangular cross section, and good stability. Furthermore, we obtained high quality single mode lasing with a low threshold and a high quality factor of  $\sim 3000$  from the CsPbBr<sub>3</sub> MWs under optical pumping at room temperature. Moreover, we converted CsPbBr<sub>3</sub> MWs into CsPbCl<sub>x</sub>Br<sub>3-x</sub> ( $0 < x < 2$ ) MWs via gas phase anion exchange. By controlling the reaction time, we flexibly defined the Br/Cl ratio in CsPbCl<sub>x</sub>Br<sub>3-x</sub> MWs. More importantly, the single-mode lasing wavelength from CsPbCl<sub>x</sub>Br<sub>3-x</sub> MWs can be tuned from 546.8 nm to 468.0 nm. These exciting results not only pave the way for obtaining wavelength-tunable single-mode lasing but also promote the potential of lead halide perovskite applications in photoelectric devices and color displays.

The CsPbBr<sub>3</sub> MWs were prepared by a typical solvent method as shown in Fig. 1(a). In brief, a certain amount of 0.3 M CsBr and PbBr<sub>2</sub> precursor solution was added dropwise onto a piece of Si/SiO<sub>2</sub> substrate. Then, the substrate was transferred into a hermetically sealed 100 ml beaker containing 20 ml CH<sub>3</sub>CN and reacted for 24 h at 50 °C. As a result, CsPbBr<sub>3</sub> MWs with the length ranging from dozen to several hundred micrometers and the diameters in the range of 1.0–9.0 μm are obtained as shown in Figs. 1(b) and S1. In the preparing processes, some CsPbBr<sub>3</sub> nanoplates were obtained as well. The SEM images [Figs. 1(c), inset and S2] of the as-prepared CsPbBr<sub>3</sub> MWs indicate that the MWs possess a smooth surface and rectangular cross section. These expected characteristics provide a platform for the high-quality WGM lasers. The energy dispersive X-ray spectroscopy (EDX) result [Figs. 1(d)–1(h)] shows that the Cs, Pb, and Br elements are uniformly distributed in the CsPbBr<sub>3</sub> MWs with a molar ratio of

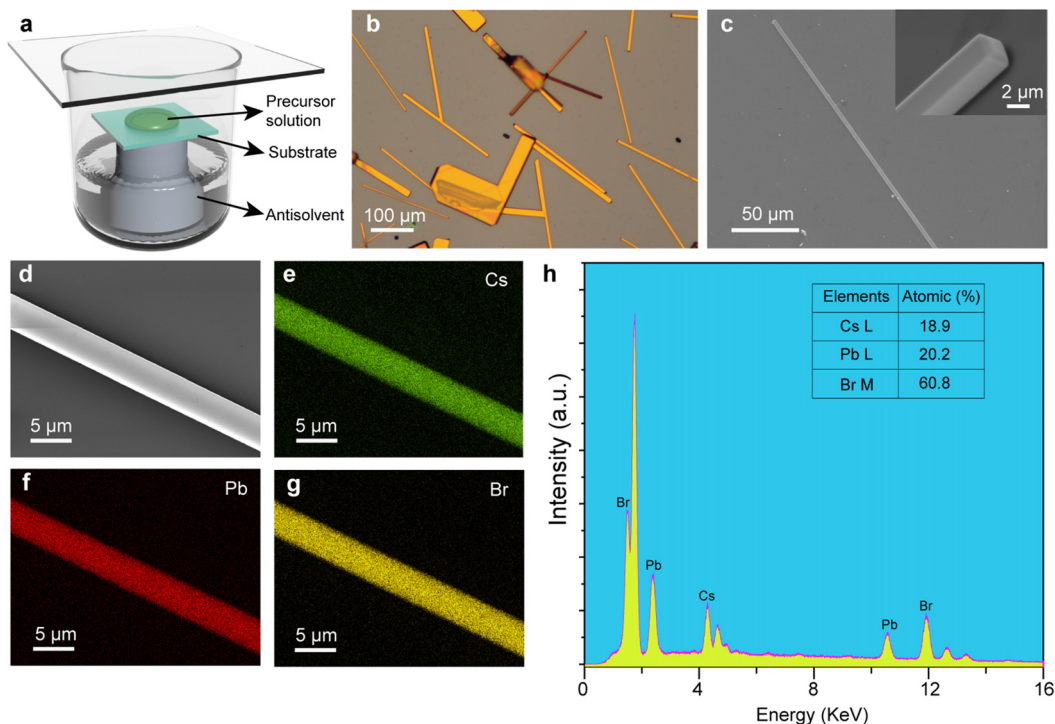


**FIG. 1.** Synthesis and morphology characterization of CsPbBr<sub>3</sub> MWs. (a) Schematic of preparing CsPbBr<sub>3</sub> MWs. The optical (b) and SEM (c) images of as-prepared CsPbBr<sub>3</sub> MWs. Inset: cross-sectional image of CsPbBr<sub>3</sub> MW. (d)–(g) The element mappings of Cs, Pb, and Br distribution in CsPbBr<sub>3</sub> MWs and the corresponding energy dispersive X-ray spectroscopy (EDX) spectrum (h).

approximately 1:1:3, which is agreement with the stoichiometry of  $\text{CsPbBr}_3$ .

To study the crystal structure of the as-prepared  $\text{CsPbBr}_3$  MWs, we conducted the X-ray diffraction (XRD) measurement as shown in Fig. 2(a). In general,  $\text{CsPbBr}_3$  refers to the orthorhombic phase at the low growth temperature ( $50^\circ\text{C}$ ). Two clear splitting peaks appeared at  $15.4^\circ$  and  $30.9^\circ$ , which correspond to 110 and 220 lattice planes of orthorhombic phase  $\text{CsPbBr}_3$ , respectively. The XRD result demonstrates that the as-prepared  $\text{CsPbBr}_3$  MWs belong to the orthorhombic phase (space group  $Pbnm$ ). Figure 2(b) shows the photoluminescence (PL, red line) spectrum of  $\text{CsPbBr}_3$  MWs. It can be seen that the PL peak is located at  $529.0\text{ nm}$  with a narrow full width at half maximum (FWHM) of about  $18.0\text{ nm}$ , indicating that our  $\text{CsPbBr}_3$  MWs possess good crystalline quality.

The examination of all laser properties of  $\text{CsPbBr}_3$  MWs is conducted on a home-built  $\mu$ -PL system as shown in Fig. 3(a). The excitation source was a femtosecond pulsed laser with a  $355\text{ nm}$  wavelength, a  $190\text{ fs}$  pulse duration, and a  $1\text{ kHz}$  repetition frequency. Following that, the laser beam was focused on the sample by a  $\times 40$  objective (the diameter of the laser spot is  $\sim 30.0\text{ }\mu\text{m}$ ). Figure 3(b) shows the pump-dependent PL spectra of a single  $\text{CsPbBr}_3$  MW with a diameter of  $3.1\text{ }\mu\text{m}$ . It can be seen that the PL displays a broad spontaneous emission peak when the pump fluence is below  $9.1\text{ }\mu\text{J cm}^{-2}$ . However, when the pump fluence is above  $9.1\text{ }\mu\text{J cm}^{-2}$ , a narrow sharp peak emerges at a wavelength of  $546.0\text{ nm}$ , and the emission intensity is dramatically enhanced with the increase in pump fluence, indicating the occurrence of lasing behavior. The inset shows the brightness field (top) and dark field (middle and bottom) fluorescence photographs of the single  $\text{CsPbBr}_3$  MW. At a low pump fluence, the  $\text{CsPbBr}_3$  MW presents the uniform green fluorescence at the excited section. Once the pump fluence exceeds the threshold, a typical lasing phenomenon appeared, which also demonstrates the occurrence of lasing behavior. The quality factor ( $Q$ ) is an important indicator for the laser; here, the lasing  $Q$  is calculated by the following formula:

$$Q = \lambda / \Delta\lambda, \quad (1)$$

where  $\lambda$  is the resonant wavelength of lasing mode and  $\Delta\lambda$  is the FWHM of the emitted lasing. Figure 3(c) shows that the Gaussian fitted lasing peak at the pumping fluence is  $9.2\text{ }\mu\text{J cm}^{-2}$  with a FWHM

of  $0.18\text{ nm}$ , and the calculated  $Q$  value is  $\sim 3000$ . It is notable that the value of the  $Q$  factor is comparable with that of  $\text{CsPbBr}_3$  NW lasers prepared by CVD. Figure 3(d) shows the log–log plotted output intensity (red sphere) and FWHM (blue sphere) vs pumping fluence. The plotted curve profile shows an expected “S”-shape, implying the occurrence of lasing behavior.<sup>35,36</sup> The first kink appeared at a pumping fluence of  $9.1\text{ }\mu\text{J cm}^{-2}$ , suggesting that the laser pumping threshold ( $P_{\text{th}}$ ) of the  $\text{CsPbBr}_3$  NW is  $9.1\text{ }\mu\text{J cm}^{-2}$ .<sup>36</sup> Moreover, it also demonstrated the transition from spontaneous emission to stimulated radiation with the increase in pumping fluence. Previous studies demonstrated that the lasing resonant mode in the  $\text{CsPbBr}_3$  MW with a rectangular cross section should be ascribed to WGM mode.<sup>15,34</sup> The inset in Fig. 3(d) presents the schematic diagram of the waveguide in the  $\text{CsPbBr}_3$  NW cross section. We also tested a series of  $\text{CsPbBr}_3$  MWs with different diameters as shown in Fig. S3. It can be seen that the lasing from single mode turn to dual-mode with the diameter of  $\text{CsPbBr}_3$  MW increases from  $3.1\text{ }\mu\text{m}$  to  $4.7\text{ }\mu\text{m}$ . With a further increase in the diameter, the free spectral space (FSR) decreases, which is attributed to the large cross-sectional area, allowing for the existence of higher-order modes. One important merit of all-inorganic perovskites is their superior stability compared with the organic–inorganic perovskite. The stability test of the  $\text{CsPbBr}_3$  NW performed at pumping fluence is  $1.2 P_{\text{th}}$  as shown in Fig. 3(e). Interestingly, the PL intensity of the  $\text{CsPbBr}_3$  MW has no obvious decay even after continuing excited for 100 min, indicating a good stability.

Gas-phase anion exchange is a facile and controllable method to prepare  $\text{CsPbCl}_x\text{Br}_{3-x}$  alloys. Figure 4(a) shows the diagram of gas-phase anion exchange in this work. In brief, the as-prepared  $\text{CsPbBr}_3$  MWs were transferred into a  $\Phi = 150\text{ mm}$  crystallizing dish containing a certain amount of hydrochloric acid and anhydrous calcium chloride. Next, the reaction system was transferred into a stove and maintained at  $60^\circ\text{C}$  for hours. Here,  $\text{CaCl}_2$  is used to reduce humidity, and hydrochloric acid serves as the  $\text{Cl}^-$  resource. The roughness of the sample surface has a great influence on the lasing quality. Previous reports have shown that the surface smoothness of the perovskite is affected by the rate of anion exchange due to the decrease in lattice parameters when  $\text{Br}^-$  is substituted by  $\text{Cl}^-$ .<sup>11</sup> Therefore, it is necessary to explore a suitable condition for anion exchange. Figure S4(a) shows the SEM image of  $\text{CsPbCl}_x\text{Br}_{3-x}$  MW after reaction for 8 h with

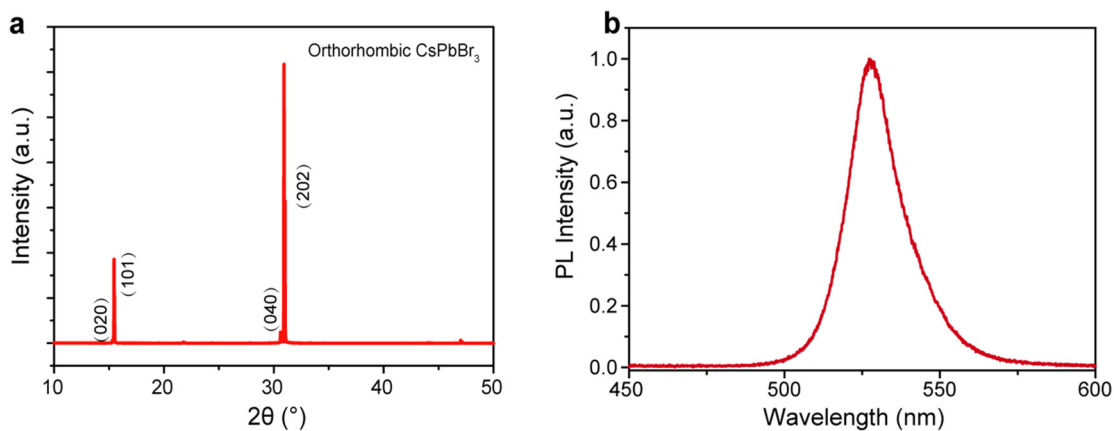
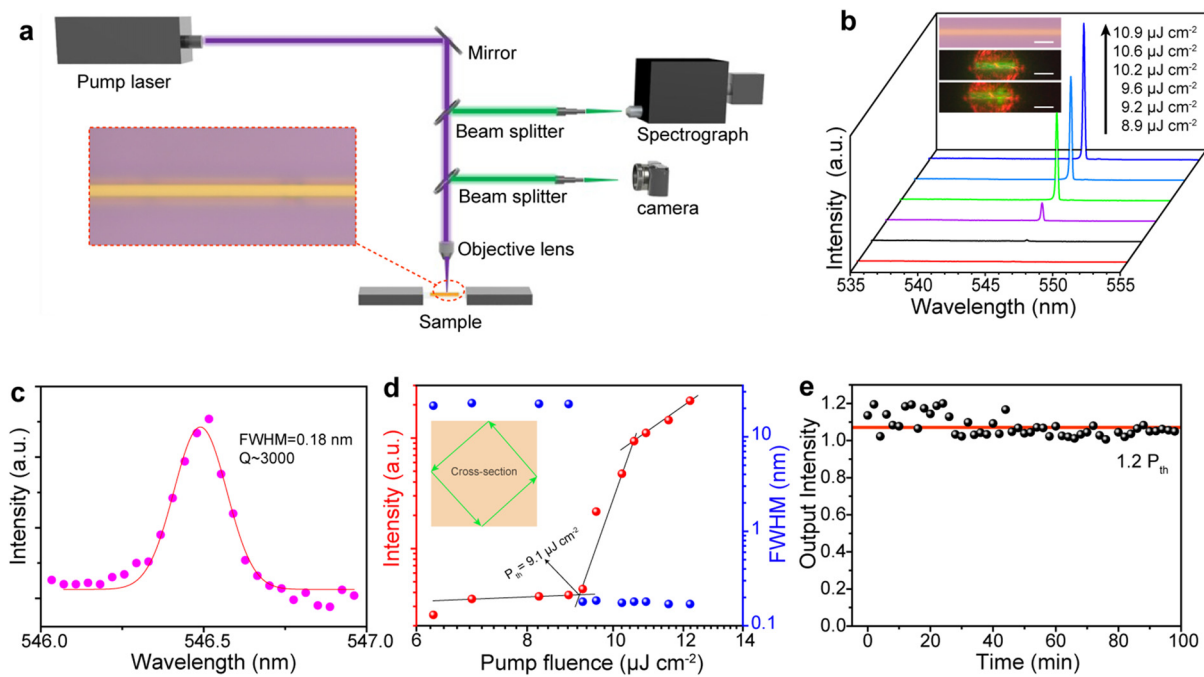


FIG. 2. (a) XRD pattern of  $\text{CsPbBr}_3$  MWs. (b) The PL spectrum of  $\text{CsPbBr}_3$  MWs.



**FIG. 3.** Lasing property characterization of CsPbBr<sub>3</sub> MWs. (a) Schematic diagram of the  $\mu$ -L system. (b) The PL spectra with the pump fluence increasing. Inset: bright (top) and dark (middle and bottom) field fluorescent images of the CsPbBr<sub>3</sub> MW. (c) A Gaussian fitted lasing peak at a pumping fluence of  $9.2 \mu\text{J cm}^{-2}$  showed that the FWHM is 0.18 nm. (d) The plots of output intensity and FWHM as function vs pump intensity. (e) The stability measurement under  $1.2 P_{th}$ .

150  $\mu\text{l}$  hydrochloric acid. It is clear that the MW has been broken and there are many cracks on the surface. When the hydrochloric acid amount decreased to 100  $\mu\text{l}$ , the cracks disappear and also breakage emerges. Fortunately, when the amount of hydrochloric acid decreased

to 50  $\mu\text{l}$ , the morphology of the MW still remained very well even after reaction for 8 h; neither breaking occurred nor cracks emerged. This phenomenon is attributed to the decrease in the hydrochloric acid amount, leading to the decrease in the concentration of HCl (gas) and

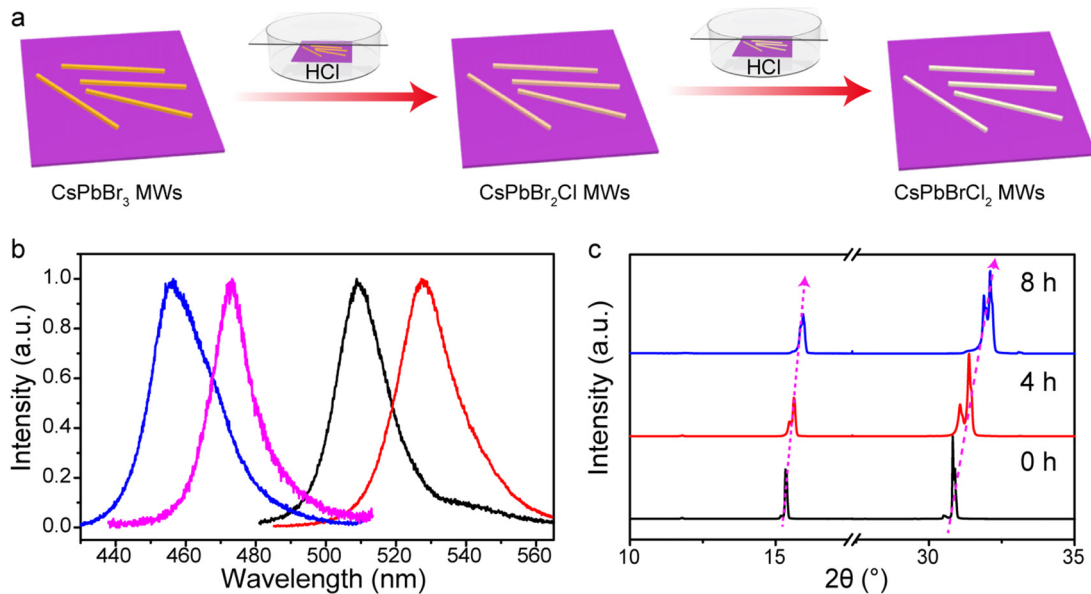


**FIG. 4.** Gas-phase anion exchange process. (a) Schematic diagram of preparing CsPbCl<sub>x</sub>Br<sub>3-x</sub> MWs by the gas-phase anion exchange method. (b) The PL spectra of CsPbCl<sub>x</sub>Br<sub>3-x</sub> MWs with the Cl element increasing. (c) XRD patterns of CsPbCl<sub>x</sub>Br<sub>3-x</sub> MWs.

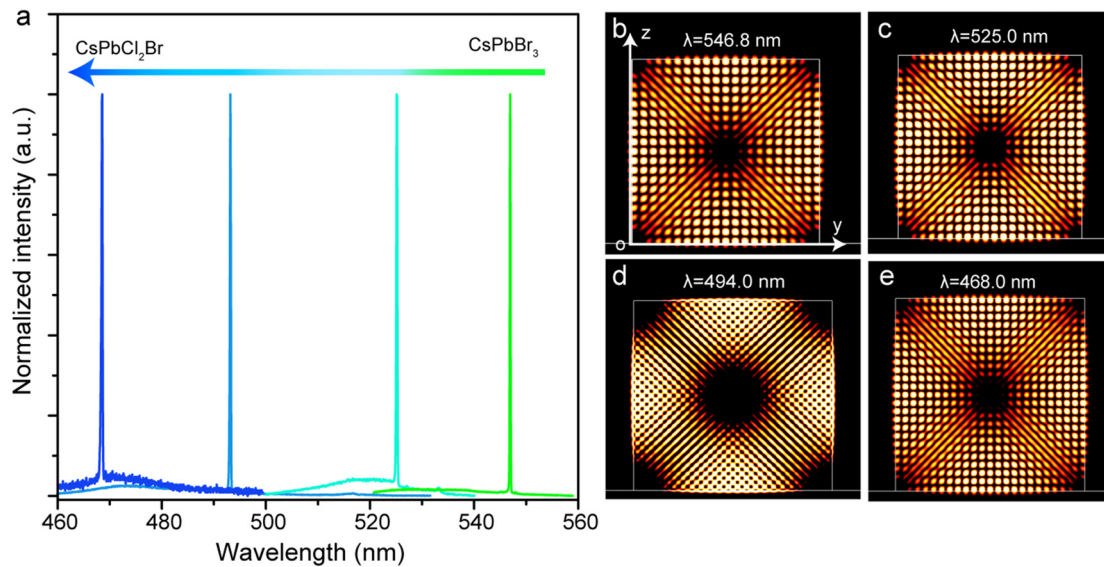


**FIG. 5.** (a) The multiwavelength lasing spectra from CsPbCl<sub>x</sub>Br<sub>3-x</sub> MWs. (b)–(e) The 2D electric field intensity distribution in the CsPbCl<sub>x</sub>Br<sub>3-x</sub> MW cross section with the emitted lasing wavelength shift from 546.8 nm to 468.0 nm, respectively.

slowing down of the anion exchange rate. Figure 4(b) shows the PL spectra of CsPbCl<sub>x</sub>Br<sub>3-x</sub> MW after anion exchange reaction for different times. We found that the PL peaks of the CsPbCl<sub>x</sub>Br<sub>3-x</sub> MW (are) gradually shift from 528 nm to 453 nm as the reaction time increases. It is ascribed to the enlarged bandgap of the lead halide perovskite when the Br<sup>-</sup> is substituted by Cl<sup>-</sup>. Therefore, the blue shift of PL peaks also indicates that the ratio of Br/Cl in CsPbCl<sub>x</sub>Br<sub>3-x</sub> MW alloys decreases with the continuity of the reaction. According to previous reports,<sup>27,28,37</sup> the PL located at 456 nm corresponding to the chemical composition in the cesium lead halide perovskite is CsPbCl<sub>2</sub>Br. Figure 4(c) shows the XRD patterns of CsPbCl<sub>x</sub>Br<sub>3-x</sub> MW in different reaction stages. There are two clear splitting peaks appearing at all samples, which correspond to the 110 and 220 lattice planes of the orthorhombic phase perovskite. Moreover, the two peaks gradually shift to a high angle with the increase in the Cl content, leading to a decrease in lattice parameters when Br<sup>-</sup> is substituted by Cl<sup>-</sup>. Combining PL spectra with XRD results, we can conclude that the CsPbBr<sub>3</sub> MWs transform into CsPbCl<sub>2</sub>Br MWs after the anion exchange reaction.

Furthermore, we studied the laser performance of CsPbCl<sub>x</sub>Br<sub>3-x</sub> MW alloys in the aforementioned  $\mu$ -PL system as shown in Fig. 5(a). All the samples presented a sharp lasing peak, indicating the occurrence of lasing behavior. The lasing peaks gradually shift from 546.8 nm to 468.0 nm with the Cl<sup>-</sup> content increasing due to the enlarged bandgap. The dark field photographs intuitively show the laser color change from green to blue as shown in Fig. S5(a). In addition, we collected the lasing spectra of CsPbCl<sub>x</sub>Br<sub>3-x</sub> MWs at different anion exchange reaction times as shown in Figs. S5(b) and S5(c). The lasing wavelength can be controlled by the anion exchange reaction time, and the smallest step is about 8.0 nm. To confirm the microcavity mode with the lasing wavelength shift from 546.8 nm to 468 nm, we have performed the simulation of the two-dimensional (2D) electric field intensity distribution in the CsPbCl<sub>x</sub>Br<sub>3-x</sub> MWs cross section

by the finite difference time domain (FDTD) as shown in Figs. 5(b)–5(d). The pattern of simulation clearly demonstrated that the light field was efficiently confined in the cross section by total reflection at the edge, suggesting a typical WGM mode cavity. All results proved that we have obtained a tunable wavelength single-mode laser from CsPbCl<sub>x</sub>Br<sub>3-x</sub> MW by gas-phase anion exchange. Our results are helpful for preparing the multicolor single-mode laser from the single perovskite MW.

In summary, we prepared CsPbBr<sub>3</sub> MWs by a solution method. The as-prepared CsPbBr<sub>3</sub> MWs present the excellent lasing performance with a low threshold of  $9.1 \mu\text{J cm}^{-2}$  and a high quality factor of  $\sim 3000$ . We obtained CsPbCl<sub>x</sub>Br<sub>3-x</sub> MW alloys via the gas-phase exchange method on the premise of ensuring the crystal quality. More importantly, we realized the multiwavelength single-mode laser output from CsPbCl<sub>x</sub>Br<sub>3-x</sub> MW, and the tunable range is from 546.8 to 468.0 nm. The results promote the potential of lead halide perovskite applications in integrated photonic and optoelectronic devices.

See the [supplementary material](#) for the information about CsPbBr<sub>3</sub> MWs' growth, morphology, and lasing property characterization and anion exchange process.

The authors acknowledge the support of the National Key R&D Project from the Ministry of Science and Technology, China (Nos. 2018YFA0703702 and 2016YFA0202703); National Natural Science Foundation of China (Nos. 51971025, 61675027, 51622205, 51432005, 61805015, and 61804011); Beijing City Committee of Science and Technology (Nos. Z171100002017019 and Z181100004418004); Beijing Natural Science Foundation (Nos. 4181004, 4182080, 4184110, 2184131, and Z180011); Shenzhen Fundamental Research Project (No. JCYJ20190808170601664); and

Shenzhen Science and Technology Program (Grant No. KQTD20170810105439418).

#### DATA AVAILABILITY

The data that support the findings of this study are available within the article and its [supplementary material](#).

#### REFERENCES

- <sup>1</sup>M. Zhuge, C. Pan, Y. Zheng, J. Tang, S. Ullah, Y. Ma, and Q. Yang, *Adv. Opt. Mater.* **7**(17), 1900275 (2019).
- <sup>2</sup>L. Huang, Q. Gao, L. D. Sun, H. Dong, S. Shi, T. Cai, Q. Liao, and C. H. Yan, *Adv. Mater.* **30**(27), e1800596 (2018).
- <sup>3</sup>Y. An, X. Shen, Y. Zhang, D. Liu, Y. Wu, P. Guo, W. Zhou, and Y. Hao, *Adv. Mater. Interfaces* **7**, 1902126 (2020).
- <sup>4</sup>C. Zhang, C. L. Zou, H. Dong, Y. Yan, J. Yao, and Y. S. Zhao, *Sci. Adv.* **3**(7), e1700225 (2017).
- <sup>5</sup>Z. Yang, T. A. Owen, H. Cui, J. A. Webber, F. Gu, X. Wang, T. C. Wu, M. Zhuge, C. Williams, P. Wang, A. V. Zayats, W. Cai, L. Dai, S. Hofmann, M. Overend, L. Tong, Q. Yang, Z. Sun, and T. Hasan, *Science* **365**(6457), 1017 (2019).
- <sup>6</sup>Y. Peng, J. Lu, D. Peng, W. Ma, F. Li, Q. Chen, X. Wang, J. Sun, H. Liu, and C. Pan, *Adv. Funct. Mater.* **29**(42), 1905051 (2019).
- <sup>7</sup>Y. Liu, R. Bao, J. Tao, J. Li, M. Dong, and C. Pan, *Sci. Bull.* **65**(1), 70 (2020).
- <sup>8</sup>Y. Liu, W. Yang, S. Xiao, N. Zhang, Y. Fan, G. Qu, and Q. Song, *ACS Nano* **13**(9), 10653 (2019).
- <sup>9</sup>S. W. Eaton, A. Fu, A. B. Wong, C. Ning, and P. Yang, *Nat. Rev. Mater.* **1**(6), 1 (2016).
- <sup>10</sup>W. Ma, J. Lu, Z. Yang, D. Peng, F. Li, Y. Peng, Q. Chen, J. Sun, J. Xi, and C. Pan, *ACS Nano* **13**(5), 5049 (2019).
- <sup>11</sup>C. Pan, L. Dong, G. Zhu, S. Niu, R. Yu, Q. Yang, Y. Liu, and Z. Wang, *Nat. Photonics* **7**(9), 752 (2013).
- <sup>12</sup>J. Lu, F. Li, W. Ma, J. Hu, Y. Peng, Z. Yang, Q. Chen, C. Xu, C. Pan, and Z. L. Wang, *Adv. Sci.* **6**(22), 1900916 (2019).
- <sup>13</sup>T. Kuykendall, P. Ulrich, S. Aloni, and P. Yang, *Nat. Mater.* **6**(12), 951 (2007).
- <sup>14</sup>Z. Yang, D. Wang, C. Meng, Z. Wu, Y. Wang, Y. Ma, L. Dai, X. Liu, T. Hasan, X. Liu, and Q. Yang, *Nano Lett.* **14**(6), 3153 (2014).
- <sup>15</sup>Z. Yang, J. Lu, M. ZhuGe, Y. Cheng, J. Hu, F. Li, S. Qiao, Y. Zhang, G. Hu, Q. Yang, D. Peng, K. Liu, and C. Pan, *Adv. Mater.* **31**(18), e1900647 (2019).
- <sup>16</sup>Z. Yang, Q. Xu, X. Wang, J. Lu, H. Wang, F. Li, L. Zhang, G. Hu, and C. Pan, *Adv. Mater.* **30**(44), e1802110 (2018).
- <sup>17</sup>F. Li, J. Lu, Q. Zhang, D. Peng, Z. Yang, Q. Xu, C. Pan, A. Pan, T. Li, and R. Wang, *Sci. Bull.* **64**(10), 698 (2019).
- <sup>18</sup>K. Xia, W. Wu, M. Zhu, X. Shen, Z. Yin, H. Wang, S. Li, M. Zhang, H. Wang, H. Lu, A. Pan, C. Pan, and Y. Zhang, *Sci. Bull.* **65**(5), 343 (2020).
- <sup>19</sup>S. W. Eaton, M. Lai, N. A. Gibson, A. B. Wong, L. Dou, J. Ma, L. W. Wang, S. R. Leone, and P. Yang, *Proc. Natl. Acad. Sci. U. S. A.* **113**(8), 1993 (2016).
- <sup>20</sup>X. Wang, M. Shoaib, X. Wang, X. Zhang, M. He, Z. Luo, W. Zheng, H. Li, T. Yang, X. Zhu, L. Ma, and A. Pan, *ACS Nano* **12**(6), 6170 (2018).
- <sup>21</sup>Y. Fu, H. Zhu, C. C. Stoumpos, Q. Ding, J. Wang, M. G. Kanatzidis, X. Zhu, and S. Jin, *ACS Nano* **10**(8), 7963 (2016).
- <sup>22</sup>H. Zhou, S. Yuan, X. Wang, T. Xu, X. Wang, H. Li, W. Zheng, P. Fan, Y. Li, L. Sun, and A. Pan, *ACS Nano* **11**(2), 1189 (2017).
- <sup>23</sup>C. K. Siu, J. Zhao, Y. Wang, D. Yang, X. Xu, S. Pan, and S. Yu, *J. Phys. D* **50**(22), 225101 (2017).
- <sup>24</sup>Z. Liu, J. Yang, J. Du, Z. Hu, T. Shi, Z. Zhang, Y. Liu, X. Tang, Y. Leng, and R. Li, *ACS Nano* **12**(6), 5923 (2018).
- <sup>25</sup>B. Tang, H. Dong, L. Sun, W. Zheng, Q. Wang, F. Sun, X. Jiang, A. Pan, and L. Zhang, *ACS Nano* **11**(11), 10681 (2017).
- <sup>26</sup>N. Zhang, Y. Fan, K. Wang, Z. Gu, Y. Wang, L. Ge, S. Xiao, and Q. Song, *Nat. Commun.* **10**(1), 1770 (2019).
- <sup>27</sup>L. Dou, M. Lai, C. S. Kley, Y. Yang, C. G. Bischak, D. Zhang, S. W. Eaton, N. S. Ginsberg, and P. Yang, *Proc. Natl. Acad. Sci. U. S. A.* **114**(28), 7216 (2017).
- <sup>28</sup>M. Lai, A. Obliger, D. Lu, C. S. Kley, C. G. Bischak, Q. Kong, T. Lei, L. Dou, N. S. Ginsberg, D. T. Limmer, and P. Yang, *Proc. Natl. Acad. Sci. U. S. A.* **115**(47), 11929 (2018).
- <sup>29</sup>X. He, P. Liu, S. Wu, Q. Liao, J. Yao, and H. Fu, *J. Mater. Chem. C* **5**(48), 12707 (2017).
- <sup>30</sup>D. Pan, Y. Fu, J. Chen, K. J. Czech, J. C. Wright, and S. Jin, *Nano Lett.* **18**(3), 1807 (2018).
- <sup>31</sup>B. Tang, Y. Hu, J. Lu, H. Dong, N. Mou, X. Gao, H. Wang, X. Jiang, and L. Zhang, *Nano Energy* **71**, 104641 (2020).
- <sup>32</sup>S. Makarov, A. Furasova, E. Tiguntseva, A. Hemmetter, A. Berestennikov, A. Pushkarev, A. Zakhidov, and Y. Kivshar, *Adv. Opt. Mater.* **7**(1), 1800784 (2019).
- <sup>33</sup>X. He, P. Liu, H. Zhang, Q. Liao, J. Yao, and H. Fu, *Adv. Mater.* **29**(12), 1604510 (2017).
- <sup>34</sup>S. Wang, J. Fang, C. Zhang, S. Sun, K. Wang, S. Xiao, and Q. Song, *Adv. Opt. Mater.* **5**(21), 1700529 (2017).
- <sup>35</sup>C. Huang, C. Zhang, S. Xiao, Y. Wang, Y. Fan, Y. Liu, N. Zhang, G. Qu, H. Ji, J. Han, L. Ge, Y. Kivshar, and Q. Song, *Science* **367**, 1018 (2020).
- <sup>36</sup>W. Sun, Y. Liu, G. Qu, Y. Fan, W. Dai, Y. Wang, Q. Song, J. Han, and S. Xiao, *Nat. Commun.* **11**(1), 4862 (2020).
- <sup>37</sup>H. Du, K. Wang, L. Zhao, C. Xue, M. Zhang, W. Wen, G. Xing, and J. Wu, *ACS Appl. Mater. Interfaces* **12**(2), 2662 (2020).